Macroelement Model for In-Plane and Out-of-Plane Responses of Masonry Infills in Frame Structures

F. Di Trapani[1]; P. B. Shing, M.ASCE[2]; and L. Cavaleri[3]

Abstract: A new macroelement model is presented in this paper for the simulation of the in-plane (IP) and out-of-plane (OOP) response of infilled frames subjected to seismic actions. The model consists of two diagonal, one horizontal, and one vertical struts. Each strut is represented by two fiber-section beam-column elements. The model is able to capture the arching action of the wall under an OOP load as well as the interaction between the IP and OOP actions. The proposed modeling approach is sufficiently simple and efficient that it can be used for the static or dynamic analysis of an entire structural system. An experimental validation has been carried out. A further numerical study performed with the macroelement model has shown that wall damage due to IP loads can significantly reduce the OOP resistance of the wall, and this influence depends on the slenderness (height/thickness) of the wall. A more slender wall will suffer a more significant loss of OOP resistance. **DOI: 10.1061/(ASCE)ST.1943-541X.0001926.**

Author keywords: Masonry infills; In-plane; Out-of-plane; Arching action; Macromodel; Fiber-section elements; Concrete and masonry structures.

Introduction

Infilling steel and RC frames with unreinforced masonry walls for architectural purposes is a common construction practice in many regions of the world. Frame–infill interactions under in-plane (IP) and out-of-plane (OOP) seismic loads have been investigated in depth for more than five decades. A number of theoretical models and predictive techniques have been developed to account for the influence of infills on the overall response of framed structural systems. These models range from the simple replacement of an infill panel by one or more equivalent diagonal struts (e.g., Stafford Smith 1966; Stafford Smith and Carter 1969; Mainstone 1974; Crisafulli and Carr 2007; El-Dakhakhni et al. 2003) to detailed linear and nonlinear finite-element models (e.g., Mehrabi and Shing 1997; Shing and Mehrabi 2002; Koutromanos et al. 2011). A number of researchers have extended the original work of Stafford Smith (1966) to provide reliable estimations of the stiffening effects of infills (Papia et al. 2003; Asteris et al. 2015) and the inelastic response under monotonic loads (e.g., Saneinejad and Hobbs 1995; Panagiotakos and Fardis 1996; Žarnić and Gostič 1997) and cyclic loads (e.g., Doudoumis and Mitsopoulou 1986; Madan et al. 1997; Cavaleri et al. 2005; Cavaleri and Di Trapani 2014). In the recent past, the extensive use of nonlinear static and dynamic analyses for the assessment of the seismic performance of structural systems has created a pressing need for reliable macroelement models based on beam-column elements that can deliver the required accuracy as well as computational efficiency.

For the modeling of infilled frames, most of the research has been focused on the IP behavior of the infills. However, the ability to predict the OOP response of an infill wall and its effect on the IP behavior or vice versa is needed to properly assess the performance of a three-dimensional structure. Damage induced in an infill wall by IP seismic loads could compromise the OOP resistance and lead to wall collapse. As shown in Figs. 1(a and b), the interaction between the damage mechanisms induced by IP and OOP loads is complicated. The OOP resistance of an infill wall is governed by the arching mechanism as shown in Fig. 1(b).

Experimental studies (e.g., Dawe and Seah 1989; Angel 1994; Flanagan and Bennett 1999; Griffith and Vaculik 2007; Komaraneni and Rai 2011) have demonstrated that masonry infills can develop significant resistance against OOP actions because of the arching mechanism when they are adequately confined by a boundary frame. Many of these studies have provided the following major observations:

1. OOP resistance decreases with the square of the slenderness ratio (height/thickness) of the infill wall.
2. The arching mechanism is generated by two-way bending when the infills are well confined in both directions by the surrounding frame.
3. The IP resistance of an infill wall is influenced by the inelastic deformation in the OOP direction and vice versa.

Theories and analytical models (McDowell et al. 1956a, b; Monk 1958; Angel 1994; Bashandy et al. 1995; Klingner et al. 1996; Abrams et al. 1996) have been developed to predict the OOP load capacity of masonry infills. However, only a few recent studies have attempted to simulate the interaction of the IP and OOP responses using macroelement models. Abrams et al. (1996) proposed a simple formula to calculate the reduction of the OOP resistance of a masonry infill wall due to damage induced by IP loads. Hashemi and Mosalam (2007) proposed a three-dimensional strut-and-tie model to account for the arching action as well as the IP resistance of an infill wall. It has two diagonal struts, one in each direction. Each of the two diagonal struts is modeled by four pin-connected compression-only fiber-section beam

[1]Assistant Professor, Dept. of Structural, Building, and Geotechnical Engineering, Politecnico di Torino, 10129 Turin, Italy (corresponding author). E-mail: fabio.ditrapani@polito.it

[2]Full Professor, Dept. of Structural Engineering, Univ. of California, San Diego, La Jolla, CA 92093. E-mail: pshing@ucsd.edu

[3]Associate Professor, Dipartimento di Ingegneria Civile, Ambientale, Aerospaziale, dei Materiali, Univ. of Palermo, 90128 Palermo, Italy. E-mail: liborio.cavaleri@unipa.it

Note. This manuscript was submitted on July 11, 2016; approved on June 30, 2017; published online on November 24, 2017. Discussion period open until April 24, 2018; separate discussions must be submitted for individual papers. This paper is part of the ***Journal of Structural Engineering***, © ASCE, ISSN 0733-9445.

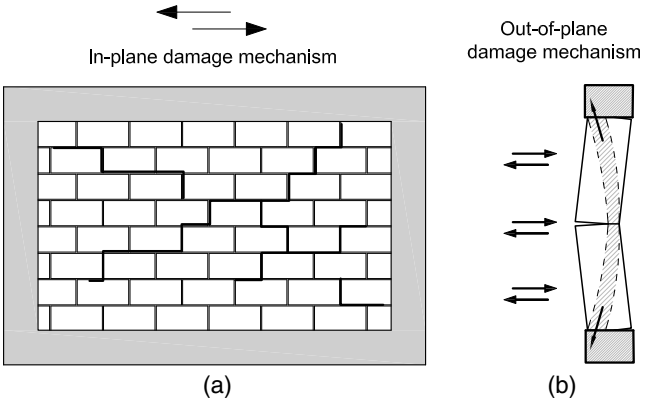

Fig. 1. Damage mechanisms of infilled frames: (a) IP; (b) OOP (arching mechanism)

elements. The midspan nodes of the diagonal struts are connected by a tension-only link in the OOP direction, forming a space truss symmetric about the middle plan of the wall. Later, Kadysiewski and Mosalam (2009) and Mosalam and Günay (2015) proposed a single-strut model consisting of two fiber-section beam-column elements connected at the midspan to account for both IP and OOP responses. The diagonal strut has tensile strength and compressive strength to provide resistance in both loading directions. The calibration of the model is performed at the fiber level by assigning different material properties to fibers at different locations in the cross section to provide the desired interaction curve for the IP and OOP load capacities.

Neither of the aforementioned models is straightforward to calibrate, so they are not easy to use. A new four-strut macroelement model that is easy to calibrate is proposed in this paper. In this model, the arching action under OOP loading is provided by fiber-section beam-column elements. The four struts can be appropriately calibrated to account for the IP and OOP responses and their interaction. The model has been validated by experimental data available in the literature.

Proposed Four-Strut Macroelement Model

The macroelement model proposed here for unreinforced masonry infill walls is formulated with three basic requirements in mind. First, the model has to account for the arching action of the masonry infill [Fig. 1(b)] under OOP loads. Second, the model has to account for the interaction between the IP and OOP actions, i.e., it has to account for the influence of wall damage caused by IP loading on the OOP response and vice versa. Lastly, the model has to be simple enough that it can be used in practice for the static or dynamic analysis of a complete structural system.

To meet the aforementioned requirements, a four-strut model is used to represent the behavior of the masonry infill, with each strut consisting of two fiber-section beam-column elements, as shown in Fig. 2. Since masonry is weak in tension, these struts do not transmit tension and are pin-connected to the frame members. The diagonal struts are used to model the IP resistance of the infill wall, which also accounts for the nonlinear behavior introduced by the frame–wall interaction, while all four struts contribute to the OOP resistance. The horizontal and vertical struts, because of their orientations, do not influence the IP response. To simulate the loss of contact between the infill and the frame during IP loading, the diagonal struts are connected to the frame through gap elements at the top (Fig. 2), which have zero tensile resistance but allow the transfer of compressive stress. For a fiber-section beam element, the internal force increment $\dot{\boldsymbol{s}}^s(x)$ at a section can be related to the increment of the section deformation, $\dot{\boldsymbol{e}}^s(x)$, through the tangent stiffness matrix $\boldsymbol{k}_T^s(x)$, where a superposed dot represents the rate of change of the variable with respect to time:

$$\dot{\boldsymbol{s}}^s(x) = \begin{bmatrix} \dot{N}(x) \\ \dot{M}(x) \end{bmatrix} = \boldsymbol{k}_T^s(x) \begin{bmatrix} \dot{\varepsilon}_0 \\ \dot{\kappa} \end{bmatrix} = \boldsymbol{k}_T^s(x)\dot{\boldsymbol{e}}^s(x) \tag{1}$$

where $\dot{\varepsilon}_0$ = axial strain rate at centroidal axis of beam; $\dot{\kappa}$ = rate of change of section curvature; and $\dot{N}(x)$ and $\dot{M}(x)$ = rates of change of axial force and bending moment, respectively. After cracking, the tangent stiffness matrix is nondiagonal, and the change in the axial load and bending moment is related to the change in the axial strain and curvature as follows:

$$\begin{aligned} \dot{N}(x) &= k_{T,11}^s \dot{\varepsilon}_0 + k_{T,12}^s \dot{\kappa} \\ \dot{M}(x) &= k_{T,21}^s \dot{\varepsilon}_0 + k_{T,22}^s \dot{\kappa} \end{aligned} \tag{2}$$

The section stiffness and resistance can be calculated with the uniaxial stress–strain relation specified for each fiber in the section. A sample fiber section for a strut model is shown in Fig. 3. Cracking will shift the neutral axis of bending, as illustrated in Fig. 3, and thus introduce an element elongation along the centroidal axis,

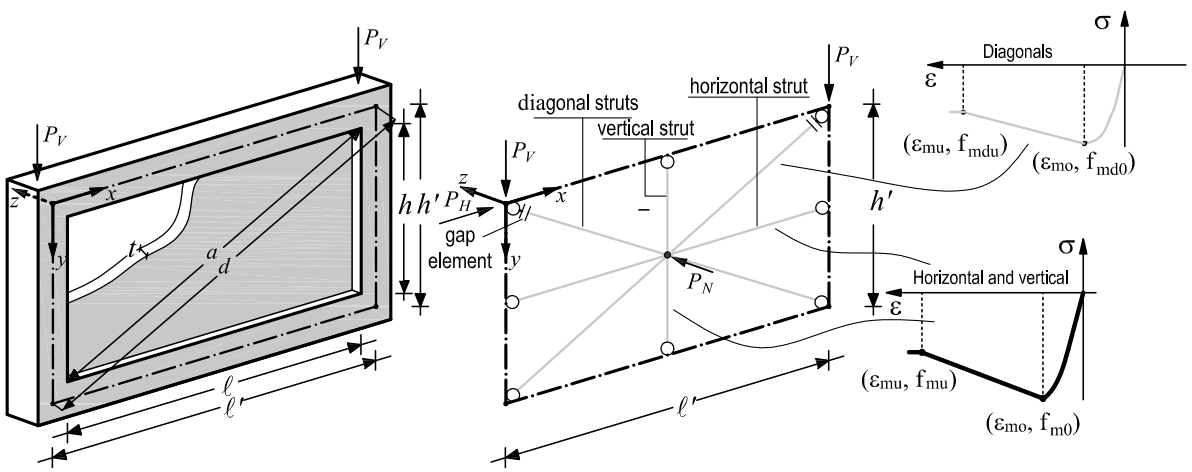

Fig. 2. Proposed four-strut macroelement model

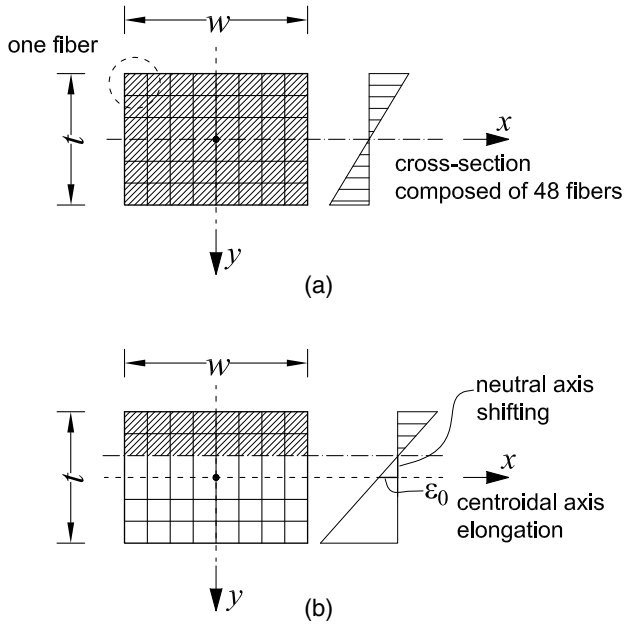

Fig. 3. Cross-section discretization: (a) uncracked section; (b) cracked section

which induces a compressive force if the two ends of the element are restrained. This feature accounts for the arching mechanism.

In the four-strut model, each strut is represented by two beam-column elements connected by a node at the midspan. Hence, four midspan nodes are introduced. These nodes are constrained to move together in the OOP direction (i.e., the z-direction shown in Fig. 2), but they move independently in IP directions. The resistance of the infill wall to IP and OOP loads and the interaction between the IP and OOP actions are determined by the strut widths and the compressive strength specified for the masonry. In this model, the width of the diagonal struts, w_d, is assumed to be one-third of the internal diagonal length a (Fig. 2), while the widths of the horizontal and vertical struts, w_h and w_v, are functions of the wall dimensions and w_d as follows:

$$w_h = h - \frac{w_d}{\cos\theta} \quad \text{and} \quad w_v = \ell - \frac{w_d}{\sin\theta} \tag{3}$$

As shown in Fig. 4, h and l are the height and the length of the wall, respectively, $w_d/\cos\theta$ is the total contact length between the diagonal struts and the columns, and $w_d/\sin\theta$ is the total contact length between with the diagonal struts and the beams. The width

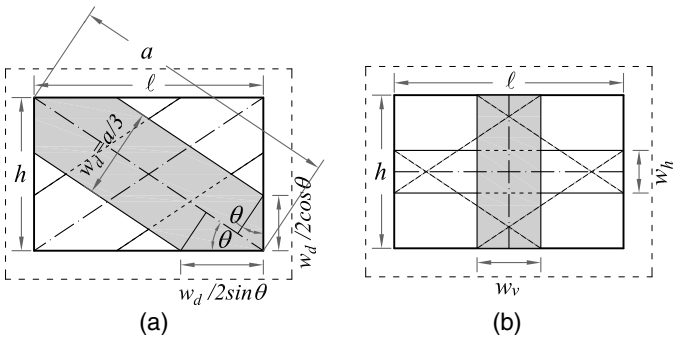

Fig. 4. Dimensions of struts: (a) diagonal struts; (b) vertical and horizontal struts

of the diagonal struts assumed here is close to the recommendations of Stafford-Smith (1966), Stafford-Smith and Carter (1969), Durrani and Luo (1994), and Papia et al. (2003). The thickness of all the struts is equal to the thickness t of the infill wall. An appropriate constitutive model has to be selected for the strut elements to represent the compressive behavior of masonry. For this purpose, the Kent–Park model (Kent and Park 1971) for concrete, as shown in Fig. 2, can be used, with the tensile strength assumed to be zero.

To accurately capture the IP and OOP resistances of the infill wall in each bay of a structure, the four-strut model is calibrated using the following procedure. First, construct the backbone curve for the IP lateral load-versus-lateral displacement response of the infilled frame representing a single bay in the structure, including the infill, the columns, and the top beam. The backbone curve can be determined with the simplified procedure and formulas recommended in Shing and Stavridis (2014) or with a pushover analysis using a detailed finite-element model when such tools are available to provide a more accurate calibration. Second, construct a beam-column element model for the single-bay infilled frame using the four-strut model to represent the infill, and calibrate the masonry material model for the diagonal struts to match the backbone curve determined previously. Alternatively, other diagonal strut models, for example the models of Panagiotakos and Fardis (1996) and Cavaleri and Di Trapani (2014), can also be used to represent the IP response of an infilled frame. However, these models must inherently account for the nonlinear behavior introduced by the frame–wall interaction as in the simplified method of Shing and Stavridis.

The effective compressive strength of masonry, f_{md0}, determined for the diagonal struts with the foregoing procedure will not necessarily represent the actual compressive strength, f_{m0}, determined from masonry prism tests, and it can be lower than the actual value. This is because the failure of a masonry infill wall can be governed by the sliding of masonry units along the bed joints rather than the crushing of masonry. Furthermore, the value of the effective compressive strength also depends on how accurate the assumed width of the diagonal struts represents the effective strut width for the infill. This process has to be repeated for each bay of the structure that has an infill with different geometric and material properties.

To calculate the OOP resistance of the infill wall, the actual compressive strength of the masonry, f_{m0}, should be used because the resistance contributed by the arching mechanism is governed by the crushing of the masonry and because the widths of the four struts represent the entire contact lengths between the infill and the frame. Since the vertical and horizontal struts provide OOP resistance only, the actual compressive strength of the masonry should be used for these struts. However, as discussed earlier, the diagonal struts assume the effective compressive strength of the masonry, f_{md0}, to represent the IP resistance of the infill. Hence, to accurately represent both the IP and OOP resistances of the infill with the effective compressive strength, the width and thickness of the diagonal struts have to be replaced by surrogate values that maintain the same cross-sectional area.

To determine the surrogate width $\tilde{w}_d$ and thickness $\tilde{t}$ of the diagonal struts, it is assumed that the OOP resistance of a strut, $q_{a,d}$, is proportional to the compressive strength of the masonry, f_{m0}, and the strut width, w_d, and is inversely proportional to the square of the slenderness ratio d/t as follows:

$$q_{a,d} \propto \frac{f_{m0} w_d}{\left(\frac{d}{t}\right)^2} \tag{4}$$

in which d is the length of the strut. The foregoing relation is supported by the test data of McDowell et al. (1956a, b), Monk (1958),

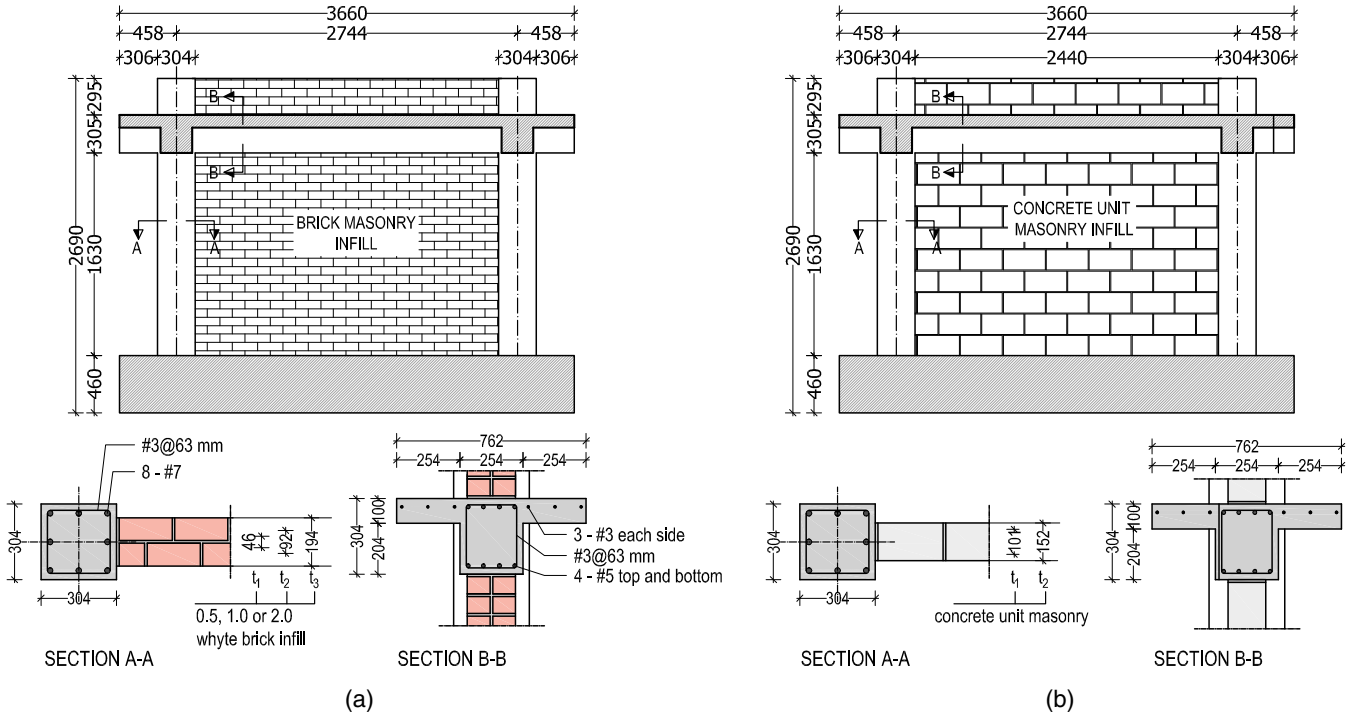

Fig. 5. Design details of infilled frames tested by Angel (1994): (a) brick masonry infill; (b) concrete unit masonry infill (dimensions in millimeters)

Angel (1994), Bashandy et al. (1995), Klingner et al. (1996), and Abrams et al. (1996) and is also validated by the numerical example presented in Appendix II. Hence, if f_{m0} is to be replaced by f_{md0} and the OOP resistance is to remain the same, the strut width w_d and thickness t have to be replaced by $\tilde{w}_d$ and $\tilde{t}$ so that

$$\frac{f_{m0} w_d}{\left(\frac{d}{t}\right)^2} = \frac{f_{md0} \tilde{w}_d}{\left(\frac{d}{\tilde{t}}\right)^2} \tag{5}$$

Furthermore, to have the correct IP resistance, the cross-sectional area of the diagonal strut has to remain unchanged, that is,

$$w_d t = \tilde{w}_d \tilde{t} \tag{6}$$

Substituting the expression for $\tilde{w}_d$ from Eq. (6) into Eq. (5) one obtains

$$\frac{f_{m0} w_d}{\left(\frac{d}{t}\right)^2} = \frac{f_{md0} w_d t}{\tilde{t}\left(\frac{d}{\tilde{t}}\right)^2} \tag{7}$$

The foregoing relation results in

$$\frac{f_{m0}}{f_{md0}} = \frac{\tilde{t}}{t} \tag{8}$$

With Eqs. (6) and (8), the surrogate cross-sectional dimensions can be determined as follows:

$$\tilde{t} = \frac{f_{m0}}{f_{md0}} t \quad \text{and} \quad \tilde{w}_d = \frac{f_{md0}}{f_{m0}} w_d \tag{9}$$

When the struts are slender, the consideration of geometric nonlinearity can be important. This can be modeled with beam-column elements formulated with the corotational coordinate transformation, in which the local coordinate system of the element moves and rotates with the element to account for the large-displacement effect. The element nodal forces and stiffness matrix in the global coordinate system are calculated with the updated local coordinates.

The proposed modeling method can be applied with a nonlinear frame analysis program, and the calibration procedure for the strut model can be programmed so that it will be easier to use in engineering practice.

Validation Analyses

The proposed model has been validated with experimental data available in the literature. Data on the OOP tests of infill walls are very limited, and some of these tests did not have severe damage induced in the walls. The model calibration and comparison with the available test data are presented below.

Masonry Infills in RC Frames

Angel (1994) tested several full-scale, single-story, single-bay RC infilled frames with IP and OOP loads. One set of specimens had brick masonry for the infill walls, and the other had solid concrete masonry units. The specimens were first subjected to IP cyclic lateral displacements until the infills reached first cracking. Then the masonry infills were subjected to a monotonically increasing pressure in the OOP direction using an air bag. The design details of the specimens are shown in Fig. 5, and the geometric and material properties for the masonry infills are presented in Table 1, in which the original nomenclature for the specimens is used.

The numerical simulations using the macroelement model were carried out with the software platform *OpenSees* using fiber-section beam-column elements with distributed plasticity. The same loading protocols used in the tests are used in the analyses. The IP lateral displacement is applied at the upper nodes of the frame model, and the OOP load is applied at the midspan nodes of the struts representing the infill.

Table 1. Geometric and Material Properties of Masonry Infills of Specimens Tested by Angel (1994)

Specimen	Infill type	Mortar type	E_m (MPa)	G_m (MPa)	f_m (MPa)	h/t	t (mm)
2	Brick	N	8,040	3,162	10.85	34.2	47.6
3	Brick	Lime	5,208	1,743	10.13	34.2	47.6
4	Concrete unit	N	12,429	1,033	22.90	17.7	92.0
5	Concrete unit	N	11,616	4,306	22.82	11.4	143.0
6	Brick	Lime	2,136	861	4.60	16.6	98.4

The material parameters for the diagonal struts, namely, f_{md0}, f_{mdu}, ε_{mo}, and ε_{mu}, as defined in Fig. 2, are calibrated using the procedure described in the previous section. In lieu of the experimental IP load-displacement curves, the backbone curves determined using the method proposed by Shing and Stavridis (2014) with modifications suggested by Di Trapani (2014) for weak infills are used for the calibration. A sample calibration of the diagonal struts for Specimen 2 is described in detail in Appendix I. However, this procedure may result in a slightly higher initial stiffness than the experimental results. In that case, the initial stiffness of the struts is lowered by increasing the strain at the peak stress (ε_{mo}) in the model. The pushover curves obtained with the method proposed by Shing and Stavridis (2014) and with the *OpenSees* model are compared to the test results in Fig. 6. The material properties and the dimensions of the diagonal, vertical, and horizontal struts determined are presented in Tables 2 and 3. The vertical and horizontal struts are relatively slender as compared to the diagonal struts with the surrogate thickness, $\tilde{t}$, and are therefore represented by elements with the corotational transformation.

The IP displacement history applied is shown in Fig. 7, in which Δ_{cr} is the displacement at first cracking in the infills. The numerical results for the IP response of the different specimens are shown in Fig. 8. For each specimen, the analysis to obtain the OOP response is conducted in the same run as the IP response analysis so that the influence of the damage caused by the IP loading is accounted for. The numerical results for the OOP response are compared to the experimental results in Fig. 9. The correlation between the experimental and numerical results is reasonably good in spite of the simplicity of the model. The difference between the experimentally and numerically obtained maximum OOP loads is between 15 and 20%. Specimens 4 and 5 were not loaded to reach the maximum OOP capacities of the infills in the tests because of the load limit of the air bag. Fig. 9(b) shows the OOP resistances contributed by the diagonal struts and the horizontal and vertical struts. It can be

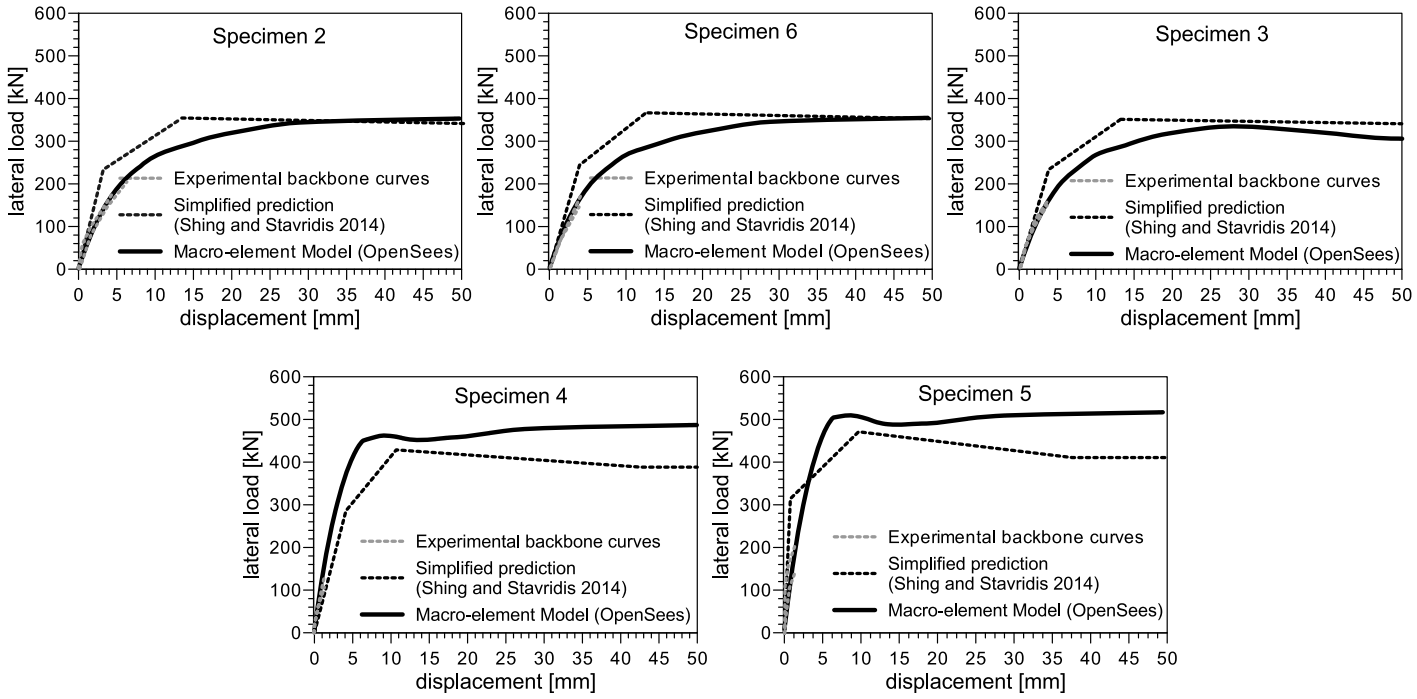

Fig. 6. Calibration of macroelement models for IP response of specimens tested by Angel (1994)

Table 2. Geometric and Material Properties of Diagonal Struts for Infills Tested by Angel (1994)

Specimen	a (mm)	ℓ (mm)	h (mm)	$\tilde{w}_d$ (mm)	$\tilde{t}$ (mm)	f_{md0} (MPa)	f_{mdu} (MPa)	ε_{mo}	ε_{mu}
2	2,934.4	2,440	1,630	202.84	229.54	2.25	1.35	0.0015	0.008
3	2,934.4	2,440	1,630	217.25	214.31	2.25	1.35	0.0015	0.008
4	2,934.4	2,440	1,630	192.21	468.18	4.50	2.70	0.0010	0.008
5	2,934.4	2,440	1,630	145.73	959.78	3.40	2.04	0.0010	0.008
6	2,934.4	2,440	1,630	239.21	402.35	1.13	0.68	0.0015	0.008

Table 3. Geometric and Material Properties of Vertical and Horizontal Struts for Infills Tested by Angel (1994)

Specimen	w_v (mm)	w_h (mm)	t (mm)	f_{m0} (MPa)	f_{mu} (MPa)	ε_{mo}	ε_{mu}
2	679.2	453.70	47.6	10.85	6.51	0.0015	0.008
3	679.2	453.70	47.6	10.13	6.08	0.0015	0.008
4	679.2	453.70	92.0	22.90	13.74	0.0015	0.008
5	679.2	453.70	143.0	22.82	13.69	0.0015	0.008
6	679.2	453.70	98.4	4.60	2.76	0.0015	0.008

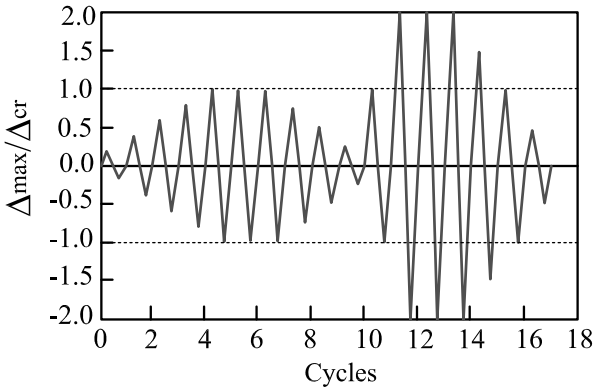

Fig. 7. IP displacement history for tests by Angel (1994)

observed that the diagonal struts provide a significant portion of the OOP resistance.

Fig. 9 also shows the OOP load capacity calculated with the formulas given in FEMA 356 (FEMA 2000) and Abrams et al. (1966). It is evident that the FEMA formula is conservative. It appears to be overly conservative, underpredicting the capacity by 50% for Specimens 2 and 3, which had infills with a high slenderness (h/t) ratio of 34.2. For Specimen 5, which had an infill with a low slenderness ratio of 11.4, the FEMA formula appears to match the numerical results well, but experimental results are not available. Similarly to FEMA 356, the strength calculated with the formula of Abrams et al. (1996) underestimates the OOP capacity of slender infills. However, for walls with lower slenderness ratios, Abrams et al.'s formula overestimates the capacity by three times.

The postpeak OOP behavior exhibited by the specimens was ductile in general. This behavior can be attributed to the two-way arching action, which allows stress redistribution. This is well captured by the model owing to the additional resistance provided by the horizontal and vertical struts, as shown in Fig. 9.

Masonry Infills in Steel Frames

Dawe and Seah (1989) and Flanagan and Bennett (1999) tested a number of masonry infilled steel frames with IP and OOP loads. The test specimens of Dawe and Seah, designated as WE2 and WE4, had a 3.6×2.8 m steel frame infilled with ungrouted concrete masonry blocks. The steel frame consisted of W250 × 58 columns, a W200 × 46 top beam, and a very stiff steel beam at the base. The design details of the specimen are shown in Fig. 10(a). No vertical loads were applied to the specimens. The OOP load was exerted by an air bag without prior IP loading. The specimens of Flanagan and Bennett, designated as S18, S19, and S25, consisted of a 2.24×2.24 m steel frame infilled with clay tile masonry. The frame had W250 × 45 columns and a W310 × 52 top

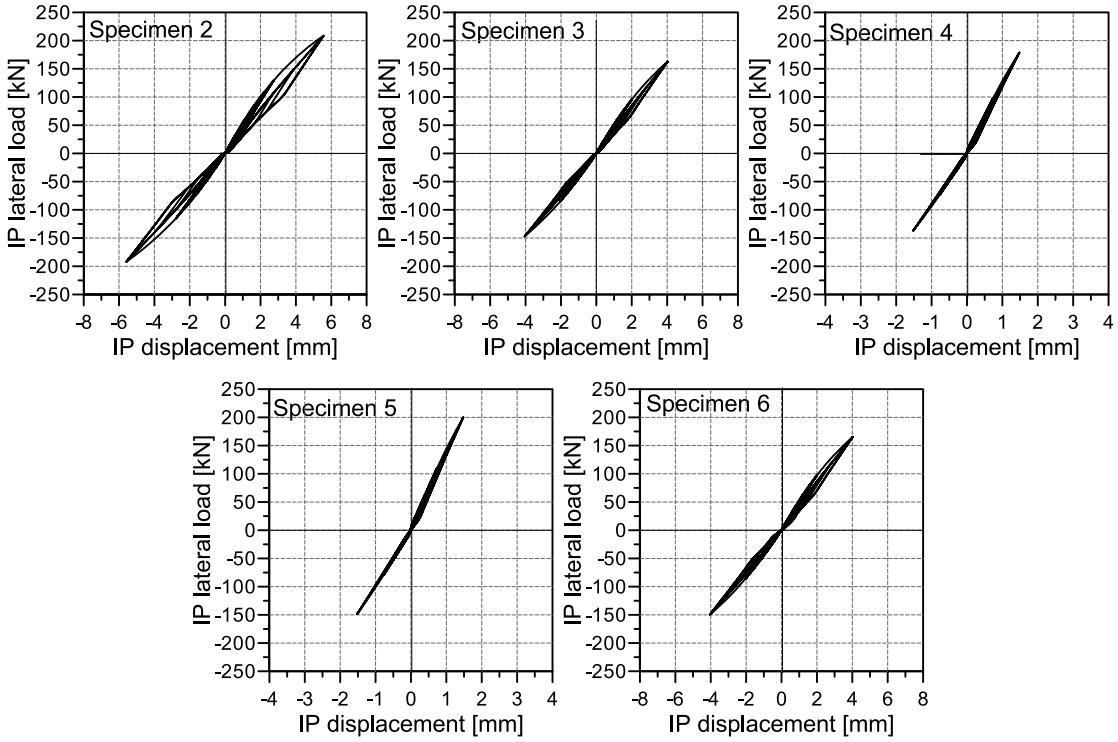

Fig. 8. Simulation of IP response of specimens tested by Angel (1994)

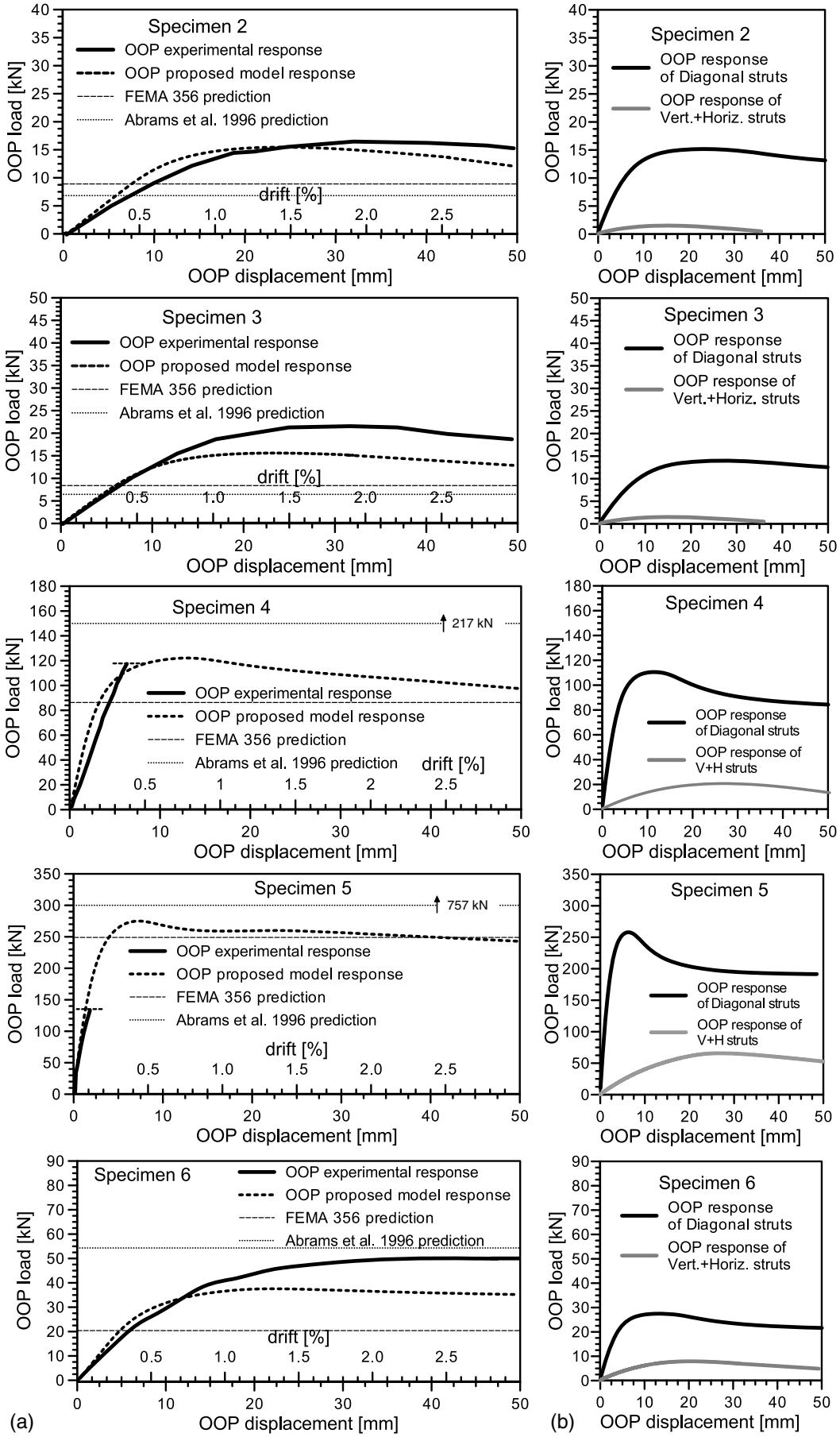

Fig. 9. Experimental and numerical results for OOP response of specimens tested by Angel (1994)

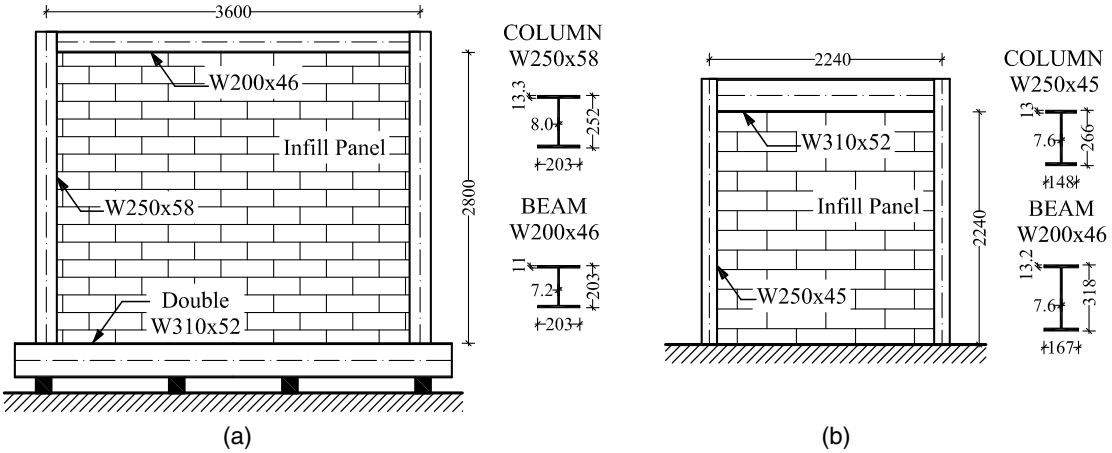

Fig. 10. Design details of specimens tested by (a) Dawe and Seah (1989); (b) Flanagan and Bennett (1999) (dimensions in millimeters)

beam. The design details of a typical specimen are shown in Fig. 10(b). No vertical loads were applied. The specimens were tested with and without prior IP loading. The OOP load was applied with cyclic loading and unloading by an air bag, and the force and midspan deflection were monitored. The geometric and material properties of all the specimens analyzed here are shown in Table 4. The struts are calibrated by the same procedure described in the previous section. The properties of the struts are presented in Tables 5 and 6.

The IP load-displacement curves obtained using the method proposed by Shing and Stavridis (2014) and the *OpenSees* model for the two sets of specimens are shown in Fig. 11. The OOP responses obtained from the tests and the *OpenSees* analyses are compared in Figs. 12 and 13. The experimental OOP response of Specimen WE4 was affected by the significant sliding of the infill wall within the frame and the twisting of the columns in the early part of the test, as reported by Dawe and Seah (1989). These phenomena are not captured by the model. To make the results comparable, the experimental response shown in Fig. 12 has the initial flat portion of the curve, caused by the sliding of the infill, removed. The experimental and numerical OOP responses show good agreement with the peak load, underestimated by the model by less than 10%. The comparison is also good for Specimen WE2, for which only the ultimate load was reported in the original study.

Specimens S18 and S19 tested by Flanagan and Bennett (1999) had the same design. Specimen S18 was tested without prior IP loading. Specimen S19 was subjected to cyclic IP loading up to

Table 4. Geometric and Material Properties of Masonry Infills of Specimens Tested by Dawe and Seah (1989) and Flanagan and Bennett (1999)

Specimen	Masonry infill type	Type of test	E_m (MPa)	f_m (MPa)	h/t	t (mm)
WE2	Concrete unit	IP: no OOP: monotonic	17,575	10.2	14.7	190
WE4	Concrete unit	IP: no OOP: monotonic	17,575	10.2	20.0	140
S18	Clay tile	IP: no OOP: cyclic	ND	5.0	11.2	200
S19	Clay tile	IP: cyclic OOP: cyclic	ND	5.0	11.2	200
S25	Clay tile	IP: no OOP: cyclic	ND	5.0	22.4	100

Note: IP = in-plane; OOP = out-of-plane; ND = not declared.

Table 5. Geometric and Material Properties of Diagonal Struts for Infills Tested by Dawe and Seah (1989) and Flanagan and Bennett (1999)

Specimen	a (mm)	ℓ (mm)	h (mm)	$\tilde{w}_d$ (mm)	$\tilde{t}$ (mm)	f_{md0} (MPa)	f_{mdu} (MPa)	ε_{mo}	ε_{mu}
WE2	4,560.7	3,600	2,800	164.00	1,762.82	1.10	0.66	0.0015	0.008
WE4	4,560.7	3,600	2,800	208.66	1,020.00	1.40	0.84	0.0015	0.008
S18/19	3,167.8	2,240	2,240	274.55	769.23	1.30	0.78	0.0015	0.008
S25	3,167.8	2,240	2,240	464.62	227.27	2.20	1.32	0.0015	0.008

Table 6. Geometric and Material Properties of Vertical and Horizontal Struts for Infills Tested by Dawe and Seah (1989) and Flanagan and Bennett (1999)

Specimen	w_v (mm)	w_h (mm)	t (mm)	f_{m0} (MPa)	f_{mu} (MPa)	ε_{mo}	ε_{mu}
WE2	1,123.8	874.07	190.0	10.20	6.12	0.0015	0.008
WE4	1,123.8	874.07	140.0	10.20	6.12	0.0015	0.008
S18/19	746.7	746.7	200.0	5.00	3.00	0.0015	0.008
S25	746.7	746.7	100.0	5.00	3.00	0.0015	0.008

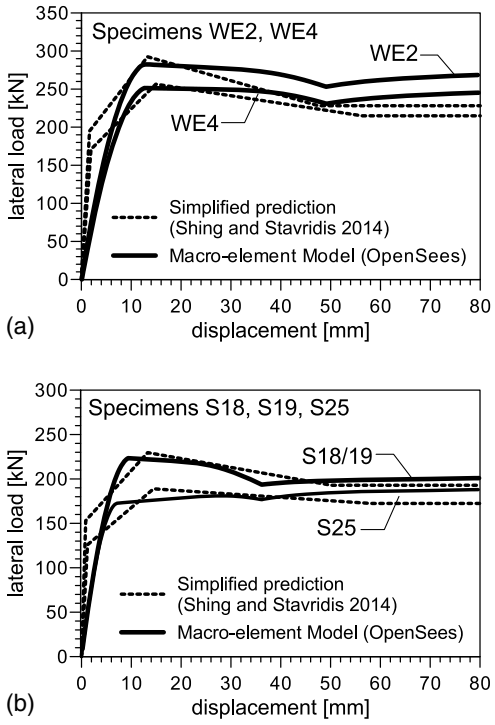

Fig. 11. Calibration of macroelement models for IP response of specimens tested by (a) Dawe and Seah (1989); (b) Flanagan and Bennett (1999)

80% of the peak load and a lateral drift of approximately 1%. The experimental and numerical results are compared in Fig. 13. For both cases, the *OpenSees* model accurately reproduces the experimental results. The effect of the damage induced by the IP load on the OOP response is well captured. The numerical response captures the initial loss and regain of stiffness due to damage caused by the IP load. This delay in the arching action was caused by the partial loss of contact between the damaged infill and bounding frame. This behavior was not evident in the specimens tested by Angel (1994), which had only mild damage induced by IP loads.

Specimen S25 tested by Flanagan and Bennett (1999) had an infill wall that was half as thick as those in Specimens S18 and S19. It was subjected to an OOP load without prior IP loading. For this specimen, only the peak OOP load and displacement were reported in the original study. As shown in Fig. 13, the numerical response slightly underestimates the peak load attained in the test.

Influence of Damage by In-Plane Load on Out-of-Plane Resistance

The influence of wall damage induced by an IP lateral load on the OOP resistance of the wall is further investigated with the macroelement strut model. For this purpose, Specimens 2 and 4 tested by Angel (1994), which had slenderness ratios of 34 and 18, respectively, are considered. In the numerical study, each of these specimens is subjected to four levels of IP displacements, with the

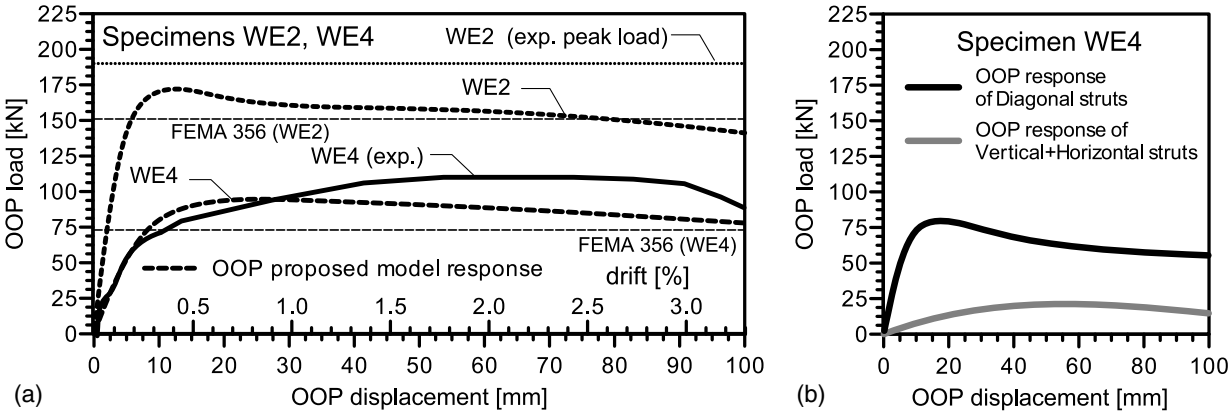

Fig. 12. Experimental and numerical results for OOP response of specimen tested by Dawe and Seah (1989)

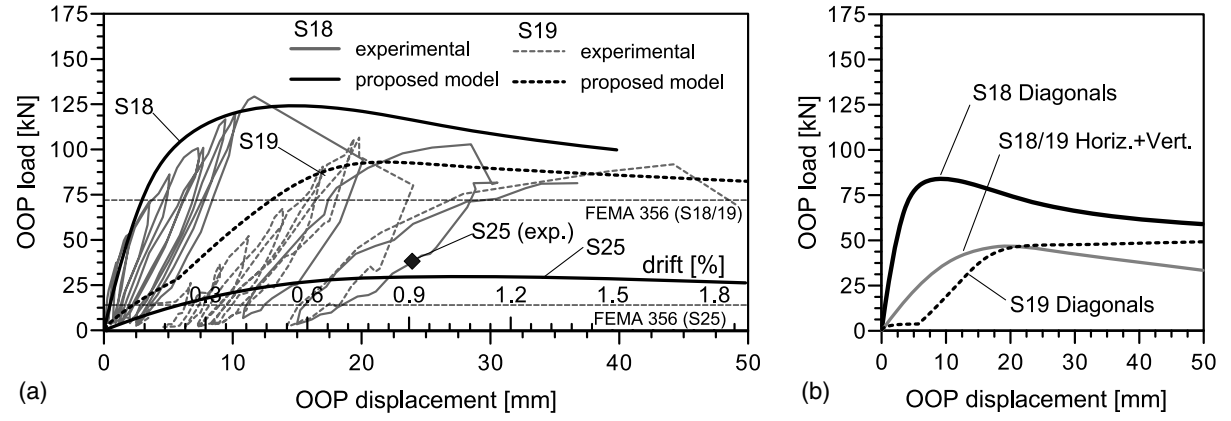

Fig. 13. Experimental and numerical results for OOP response of Specimens S18, S19, and S25 tested by Flanagan and Bennett (1999)

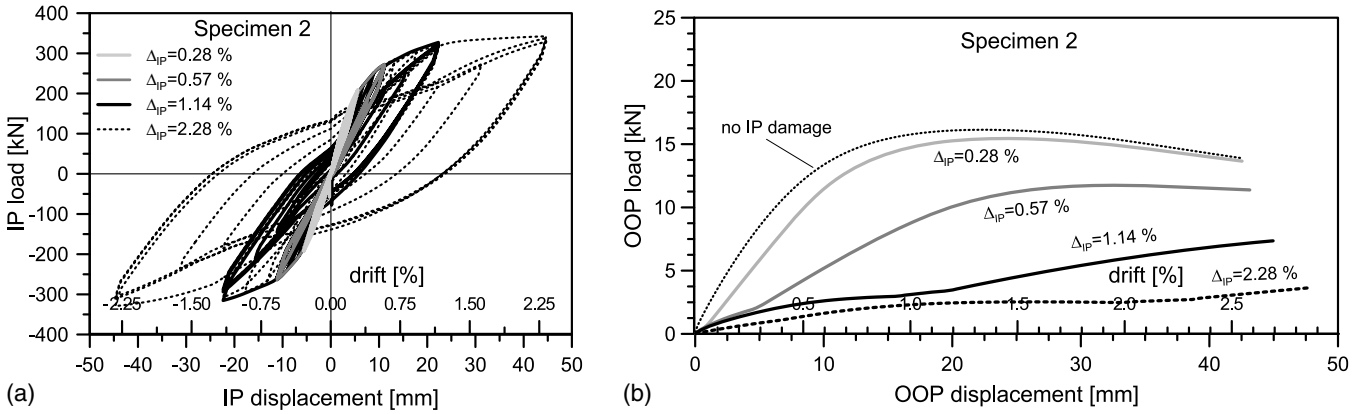

Fig. 14. OOP response of Specimen 2 tested by Angel (1994) with different levels of IP damage: (a) IP load-displacement response; (b) OOP response after IP damage

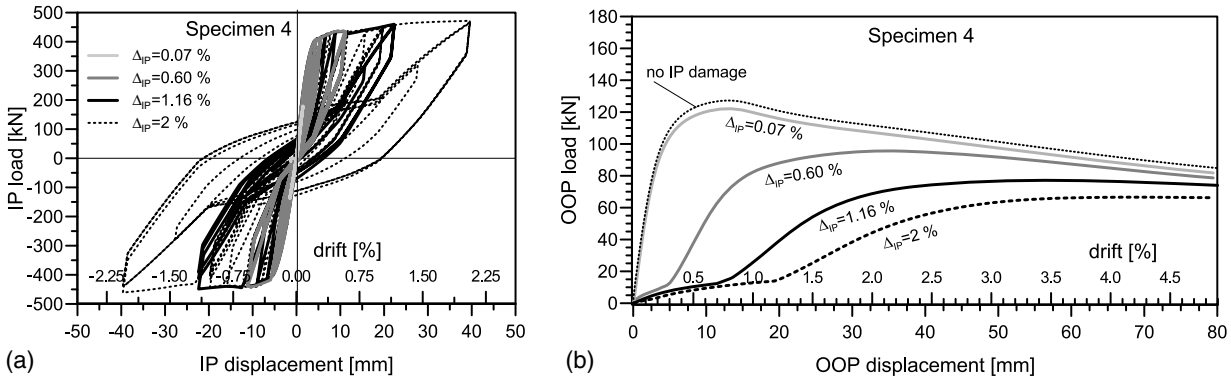

Fig. 15. OOP response of Specimen 4 tested by Angel (1994) with different levels of IP damage: (a) IP load-displacement response; (b) OOP response after IP damage

maximum story drift between 0.1 and 2.5%. After attaining each story drift level, the wall is loaded in the OOP direction to find the maximum resistance.

The IP displacement history imposed is shown in Fig. 7. The numerical results are shown in Figs. 14 and 15. It can be observed that the OOP response is strongly related to the level of the IP displacement experienced, especially for the initial portion of the OOP force-displacement curve, where the initial stiffness is significantly reduced as the wall damage due to the IP displacement increases. However, as the OOP displacement increases, the walls partially regain their OOP stiffness. This is consistent with what was observed in Specimen 19 tested by Flanagan and Bennett (1999) and can be attributed to the fact that the arching action could not be immediately engaged after the wall had been damaged. This is replicated in the macroelement model by the crushing occurring in the diagonal struts. The results shown in Figs. 14 and 15 indicate that the effect of wall damage due to IP loading is related to the slenderness (h/t) of the wall. A more slender wall suffers a more significant loss of OOP resistance for the same prior IP drift level experienced. However, as shown in Fig. 16, this is true only when the IP story drift ratio exceeds 0.75%, below which the effect of the wall damage is almost the same regardless of the slenderness ratio. Fig. 16 also shows that the loss of the OOP resistance estimated by the formula of Abrams et al. (1996) is significantly higher than that calculated using the four-strut model.

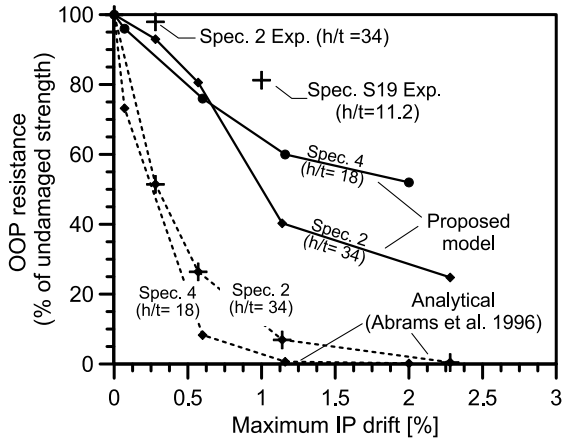

Fig. 16. Reduction of OOP load capacity of Specimens 2 and 4 tested by Angel (1994) as a function of IP story drift

Conclusions

A new four-strut macroelement model is presented in this paper to simulate the IP and OOP behavior of masonry infill walls. The struts in the macroelement are represented by fiber-section beam-column elements and are able to capture the arching action of the wall under an OOP load as well as the interaction between the IP and OOP actions. A simple calibration method is presented, and the model is sufficiently simple and efficient that it can be used for

the static or dynamic analysis of an entire structural system. The model has been validated with experimental data available in the literature.

A numerical study performed with the macroelement model has shown that wall damage due to IP loads can significantly reduce the OOP resistance of the wall, and this effect depends on the slenderness (height/thickness) of the wall. A more slender wall will suffer a more significant loss of the OOP resistance for the same prior IP story drift experienced. However, for IP story drift ratios less than 0.75%, the percentage loss of the OOP resistance does not appear to be related to the wall slenderness ratio.

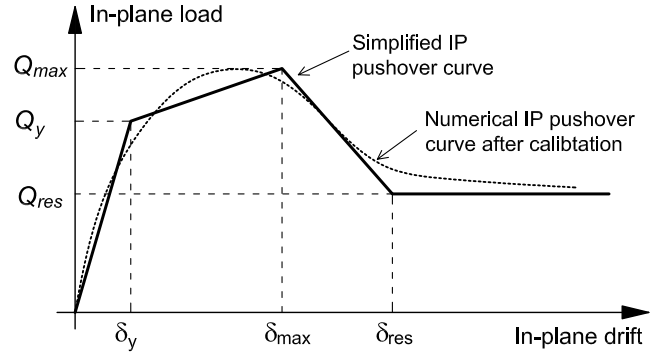

Fig. 17. Definition of simplified IP pushover curve

Appendix I. Sample Calibration of Diagonal Struts

The calibration of the diagonal struts in the macroelement model for Specimen 2 tested by Angel (1994) is presented here as an example. The first step is to construct a pushover curve for the IP response of the infilled frame using the simplified method presented in Shing and Stavridis (2014). This pushover curve has the general form shown in Fig. 17 and is characterized by six parameters, namely, $Q_{\max}$, Q_y, Q_{res}, $\delta_{\max}$, δ_y, and δ_{res}, as shown in the figure. The properties of the infilled frame and the calculation of the values of these parameters are summarized in Table 7. The reader is referred to Shing and Stavridis (2014) for a detailed explanation of the formulas presented in the table. However, the formulas

Table 7. Properties of Infilled Frame and Parameters for Pushover Curve for Specimen 2

Property	Parameter
h' (height of infilled frame)	1,930 mm
h (height of infill wall)	1,630 mm
ℓ (length of infill wall)	2,440 mm
t (thickness of infill wall)	47.6 mm
A_{sh} per unit distance (column shear reinforcement)	1,005 mm^2/m
$AR_w = \ell/h$ (wall aspect ratio)	1.37
A_w (cross-sectional area of infill wall)	1,660,144 mm^2
A_c (cross-sectional area of a column)	1,660,144 mm^2
f_c' (compressive strength of concrete)	55.12 MPa
E_c (modulus of elasticity of concrete)	37,000 MPa
f_{m0} (compressive strength of masonry)	10.85 MPa
E_m (modulus of elasticity of masonry)	5,200 MPa
G_m (shear modulus of masonry)	2,080 MPa
c_o (cohesive strength of mortar joint)	0.15 MPa
μ (coefficient of friction of mortar joint)	0.6
I_{ce} (moment of inertia of transformed section of uncracked infilled frame in terms of the elastic concrete property)	3.564×10^{12} mm^4
$K_{fl} = 3E_cI_{ce}/h'^3$ (flexural stiffness of uncracked infilled frame)	5,503,372 N/mm
$K_{fl} = 3E_cI_{ce}/h'^3$ (shear stiffness of infill wall)	148,208 N/mm
$K = 0.5 \times 1 \Big/ \left(\frac{1}{K_{fl}} + \frac{1}{K_{sh}}\right)$ (0.5 factor is to account for cracking)	72, 161 N/mm
Q_{lc} (shear strength of left column, based on Eurocode EC2)	389 kN
Q_{rc} (shear strength of right column, based on Eurocode EC2)	389 kN
P_v (total vertical compressive load on infilled frame)	444.8 kN
$P_w = P_v \frac{E_m A_w}{2E_c A_c + E_m A_w}$ (axial load on wall)	36.09 kN
$Q_{\max} = 0.4(Q_{lc} + Q_{rc}) + c_o A_w + \mu P_w$ (peak strength of infilled frame; 0.4 factor is to account for the condition that the columns will not have reached the peak strength when the infill reaches peak resistance)	350.3 kN
$SR = (c_0 A_w + \mu P_w)/[0.4(Q_{lc} + Q_{rc})]$ (strength ratio between infill and frame)	0.125
$Q_y = \frac{2}{3} Q_{\max}$ (yield strength of infilled frame)	233.5 kN
$Q_{res} = \eta Q_{\max}$ [residual strength of infilled frame according to Di Trapani (2014)]	339.3 kN
$\eta = \begin{cases} 1 - 0.25SR & (\text{for } SR < 1) \\ 0.75 & (\text{for } SR \geq 1) \end{cases}$	0.96
$\delta_{\max} = 0.86 - \frac{1}{3}\frac{AR_w}{\beta}$ [drift ratio of infilled frame at peak resistance according to Di Trapani (2014)]	0.69%
$\beta = \begin{cases} SR^{-0.5} & (\text{for } SR < 1) \\ 1.0 & (\text{for } SR \geq 1) \end{cases}$	2.83
$\delta_y = (Q_y/Kh') \times 10^2$ (drift ratio of infilled frame at yield)	0.168%
$\delta_{res} = \gamma \delta_{\max}$ [drift ratio at reaching residual strength according to Di Trapani (2014)]	2.89%
$\gamma = 4.3–0.82SR$	4.19

proposed in that study are intended for nonductile RC frames that have strong infill walls, which tend to demonstrate more brittle behavior than frames with weak infill walls. For frames with weak infill, like Specimen 2, some of the parameters have been calibrated with formulas suggested by Di Trapani (2014) Shear stregths of columns have been evaluated according to Eurocode 2 (CEN 2004) design formulas.

Properties of Diagonal Struts

Once the parameters for the pushover curve shown in Fig. 17 have been determined, the material properties of the diagonal struts are determined by trial and error so that the pushover curve obtained using the four-strut model matches that shown in the figure. The resulting values are as follows:

$$f_{md0} = 2.25 \text{ MPa}$$
$$f_{mdu} = 0.60 \times f_{md0} = 1.35 \text{ MPa}$$
$$\varepsilon_{m0} = 0.0015$$
$$\varepsilon_{mu} = 0.0080$$

It should be noted that the curve obtained using the simplified method results in a slightly higher stiffness than the experimental result. Hence, the value of the peak strain (ε_{m0}) shown above was determined with the experimental result instead.

Appendix II. Example Demonstrating Validity of Eq. (4)

The validity of Eq. (4) is demonstrated by the example problem shown in Fig. 18, in which the RC frame for the specimens of Angel (1994) is considered, and the compressive strength of the masonry, f_{m0}, and the d/t ratio for the strut are varied. The analysis is conducted with *OpenSees*. The results are plotted in Fig. 19, which shows that the OOP resistance, $q_{a,d}$, of the diagonal strut is linearly proportional to the two aforementioned parameters.

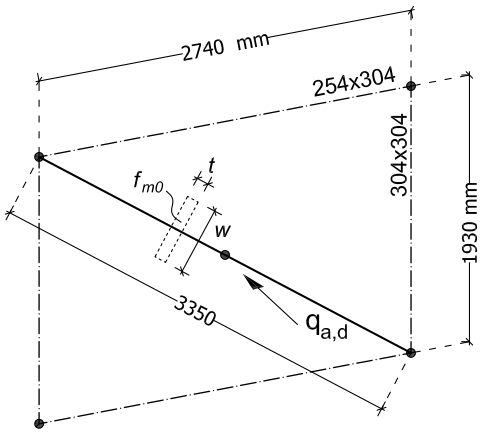

Fig. 18. Infilled frame example

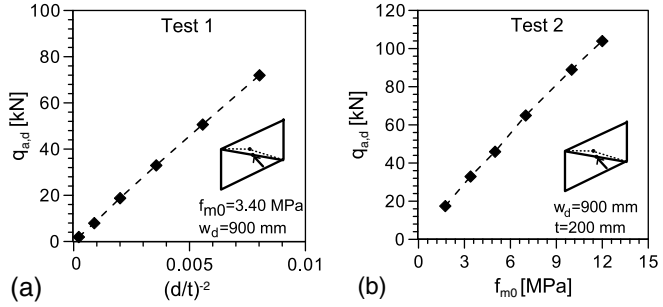

Fig. 19. Out-of-plane resistance

References

Abrams, D. P., Angel, R., and Uzarski, J. (1996). "Out-of-plane strength of unreinforced masonry infill panels." *Earthquake Spectra*, 12(4), 825–844.

Angel, R. (1994). "Behavior of reinforced concrete frames with masonry infill walls." Ph.D. thesis, Univ. of Illinois, Urbana-Champaign, IL.

Asteris, P. G., Cavaleri, L., Di Trapani, F., and Sarhosis, V. (2015). "A macro-modelling approach for the analysis of infilled frame structures considering the effects of openings and vertical loads." *Struct. Infrastruct. Eng.*, 10.1080/15732479.2015.1030761, 12(5), 551–566.

Bashandy, T., Rubiano, N. R., and Klingner, R. E. (1995). "Evaluation and analytical verification of infilled frame test data." *PMFSEL Rep. 95-1*, Phil M. Ferguson Structural Engineering Laboratory, Univ. of Texas, Austin, TX.

Cavaleri, L., and Di Trapani, F. (2014). "Cyclic response of masonry infilled RC frames: Experimental results and simplified modelling." *Soil Dyn. Earthquake Eng.*, 65, 224–242.

Cavaleri, L., Fossetti, M., and Papia, M. (2005). "Infilled frames: Developments in the evaluation of cyclic behavior under lateral loads." *Struct. Eng. Mech.*, 21(4), 469–494.

CEN (European Committee for Standardization). (2004). "Eurocode 2: Design of concrete structures. Part 1-I: General rules and rules for buildings." *EN 1992-1-1:2004*, Brussels.

Crisafulli, F. J., and Carr, A. J. (2007). "Proposed macro-model for the analysis of infilled frame structures." *Bull. N. Z. Soc. Earthquake Eng.*, 40(2), 69–77.

Dawe, J. L., and Seah, C. K. (1989). "Out-of-plane resistance of concrete masonry infilled panels." *Can. J. Civ. Eng.*, 16(6), 854–864.

Di Trapani, F. (2014). "Masonry infilled RC frames: Experimental results and development of predictive techniques for the assessment of seismic response." Ph.D. thesis, Univ. of Palermo, Palermo, Italy.

Doudoumis, I. N., and Mitsopoulou, E. N. (1986). "Non-linear analysis of multi-storey infilled frames for unilateral contact condition." *Proc., 8th European Conf. on Earthquake Engineering*, Vol. 3, Laboratório Nacional de Engenharia Civil, Lisbon, Portugal, 63–70.

Durrani, A. J., and Luo, Y. H. (1994). "Seismic retrofit of flat-slab buildings with masonry infill." *Proc., National Center for Earthquake Engineering Research Workshop on Seismic Response of Masonry Infills*, National Center for Earthquake Engineering Research, Buffalo, NY.

El-Dakhakhni, W., Elgaaly, M., and Hamid, A. (2003). "Three-strut model for concrete masonry-infilled steel frames." *J. Struct. Eng.*, 10.1061/(ASCE)0733-9445(2003)129:2(177), 177–185.

FEMA. (2000). "Prestandard and commentary for the seismic rehabilitation of buildings." *FEMA-356*, Washington, DC.

Flanagan, R. D., and Bennet, R. M. (1999). "Bidirectional behavior of structural clay tile infilled frames." *J. Struct. Eng.*, 10.1061/(ASCE)0733-9445(1999)125:3(236), 236–244.

Griffith, M. C., and Vaculik, J. (2007). "Out-of-plane flexural strength of unreinforced clay brick masonry walls." *TMS J.*, 25(1), 53–68.

Hashemi, S. A., and Mosalam, K. M. (2007). "Seismic evaluation of reinforced concrete buildings including effects of infill masonry walls." *PEER 2007/100*, Univ. of California, Berkeley, CA.

Kadysiewski, S., and Mosalam, K. M. (2009). "Modeling of unreinforced masonry infill walls considering in-plane and out-of-plane interaction." *PEER 2008/102*, Univ. of California, Berkeley, CA.

Kent, D. C., and Park, R. (1971). "Flexural members with confined concrete." *J. Struct Eng.*, 97(ST7), 1969–1990.

Klingner, R. E., Rubiano, N. R., Bashandy, T. R., and Sweenwy, S. C. (1996). "Evaluation and analytical verification of shaking table data from infilled frames. II: Out of plane behavior." *Proc., 7th North American Masonry Conf.*, Masonry Society, Boulder, CO.

Komaraneni, S., and Rai, D. C. (2011). "Seismic behavior of framed masonry panels with prior damage when subjected to out-of-plane loading." *Earthquake Spectra*, 27(4), 1077–1103.
Koutromanos, I., Stavridis, A., Shing, P. B., and Willam, K. (2011). "Numerical modelling of masonry-infilled RC frames subjected to seismic loads." *Comput. Struct.*, 89(11–12), 1026–1037.
Madan, A., Reinhorn, A. M., Mander, J. B., and Valles, R. E. (1997). "Modeling of masonry infill panels for structural analysis." *J. Struct. Eng.*, 10.1061/(ASCE)0733-9445(1997)123:10(1295), 1295–1302.
Mainstone, R. J. (1974). "Supplementary note on the stiffness and strength of infilled frames." *Current Paper CP 13/74*, Building Research Station, Watford, U.K.
McDowell, E. L., McKee, K. E., and Sevin, E. (1956a). "Arching action theory of masonry walls." *J. Struct. Div.*, 82(ST2), 915/1–915/18.
McDowell, E. L., McKee, K. E., and Sevin, E. (1956b). "Discussion of arching action theory of masonry walls." *J. Struct. Div.*, 1067, 27–40.
Mehrabi, A. B., and Shing, P. B. (1997). "Finite element modelling of masonry-infilled RC frames." *J. Struct. Eng.*, 10.1061/(ASCE)0733-9445(1997)123:5(604), 604–613.
Monk, C. B. (1958). "Resistance of structural clay masonry to dynamic forces." *Res.Rep. 7*, Structural Gay Products Research Foundation, Geneva, IL.
Mosalam, K. M., and Günay, S. (2015). "Progressive collapse analysis of RC frames with URM infill walls considering in-plane/out-of-plane interaction." *Earthquake Spectra*, 31(2), 921–943.
OpenSees [Computer software]. Pacific Earthquake Engineering Research Center, Univ. of California, Berkeley, CA.
Panagiotakos, T. B., and Fardis, M. N. (1996). "Seismic response of infilled RC frames structures." *Proc., XXI World Conf. of Earthquake Engineering*, Acapulco, Mexico.
Papia, M., Cavaleri, L., and Fossetti, M. (2003). "Infilled frames: Developments in the evaluation of the stiffening effect of infills." *Struct. Eng. Mech.*, 16(6), 675–693.
Saneinejad, A., and Hobbs, B. (1995). "Inelastic design of infilled frames." *J. Struct. Eng.*, 10.1061/(ASCE)0733-9445(1995)121:4(634), 634–650.
Shing, P. B., and Mehrabi, A. B. (2002) "Behavior and analysis of masonry-infilled frames." *Prog. Struct. Eng. Mater.*, 4(3), 320–331.
Shing, P. B., and Stavridis, A. (2014). "Analysis of seismic response of masonry-infilled RC frames through collapse." *ACI Struct. J.*, 297, 1–20.
Stafford-Smith, B. (1966). "Behavior of the square infilled frames." *Struct. Div.*, 92(1), 381–403.
Stafford-Smith, B., and Carter, C. (1969). "A method for analysis for infilled frames." *Proc., Inst. Civ. Eng.*, 7218, 31–48.
Žarnić, R., and Gostič, S. (1997). "Masonry infilled frames as an effective structural subassemblage." *Seismic design methodologies for the next generation of codes*, P. Fajfar and H. Krawinkler, eds., A.A. Balkema, Rotterdam, Netherlands, 335–346.